Supporting Information

Mid-infrared Electro-Optic Modulation in Few-layer Black Phosphorus

Ruoming Peng[1], Kaveh Khaliji[1], Nathan Youngblood[1], Roberto Grassi[1], Tony Low[11], and Mo Li[12]

[1] *Department of Electrical and Computer Engineering, University of Minnesota, Minneapolis, MN 55455, USA*

1. ***Numerical recipes*** **---** To describe the electronic energy spectrum, we use a combination of two Hamiltonians: a tight-binding model in the out-of-plane direction and a two-band $k \cdot p$ model for the in-plane. The full Hamiltonian reads as,

$$\mathrm{H} = \mathrm{H}_{\square} \otimes \mathrm{I}_{N\times N} + \mathrm{H}_{z}, \tag{S1.1}$$

where N is the number of layers. $\mathrm{H}_{\square}$ describes the low-energy electronic structure of monolayer BP around the Γ point[1],

$$\mathrm{H}_{\square} = \begin{pmatrix} \eta^{c} k_x^2 + \nu^{c} k_y^2 & \gamma k_x \\ \gamma k_x & -\eta^{v} k_x^2 - \nu^{v} k_y^2 \end{pmatrix}. \tag{S1.2}$$

The parameters $\eta^{c/v}$ and $\nu^{c/v}$ are related to in-plane effective masses of monolayer BP, via: $\eta^{c/v} = \hbar^2 / 2m_x^{c/v} \mp \gamma^2 / \Delta$ and $\nu^{c/v} = \hbar^2 / 2m_y^{c/v}$. $\Delta = 2.12$ eV is the monolayer bandgap and $\gamma = 2.84\,\mathrm{eV}\cdot \mathring{A}$ denotes intralayer conduction-valence coupling. In-plane effective masses are assumed to be $m_x^c = m_x^v = 0.15\ m_0$, $m_y^c = 0.7\ m_0$, and $m_y^v = 1.0\ m_0$, where m_0 is the free electron mass[2-4].

---

[1] Corresponding author: tlow@umn.edu

[2] Corresponding author: moli@umn.edu

H_z describes the interlayer coupling and is given by,

$$\mathrm{H}_z = \begin{pmatrix} \mathrm{H}^c & 0 \\ 0 & \mathrm{H}^v \end{pmatrix}, \tag{S1.3}$$

where each diagonal block, H^s with $s \to c/v$ for conduction/valence bands, is similar to the Hamiltonian of a linear atomic chain [4]:

$$\mathrm{H}^s = \begin{pmatrix} \varepsilon^s + \mathrm{U}_1 & \gamma^s & & \\ \gamma^s & \varepsilon^s + \mathrm{U}_2 & \ddots & \\ & \ddots & \ddots & \gamma^s \\ & & \gamma^s & \varepsilon^s + \mathrm{U}_N \end{pmatrix}. \tag{S1.4}$$

Here, $\varepsilon^{c/v} = \pm\Delta/2$ is the conduction/valence band edge in monolayer BP. We use $\gamma^c - \gamma^v = 0.88$ eV as suggested in Ref. [4]. The absolute values are then chosen such that $\gamma^c/\gamma^v = -m_z^v/m_z^c$, where $m_z^{c/v}$ is the out-of-plane effective mass of bulk BP for the conduction/valance band. The latter ensures that both the tight-binding model and effective mass approximation yield similar descriptions of energy spectrum in the bulk limit. From the values reported[2, 3] for $m_z^c = 0.2\ m_0$ and $m_z^v = 0.4\ m_0$, we have: $\gamma^c = 0.59$ eV and $\gamma^v = -0.29$ eV.

The on-site energies U_i in (S1.4) are related to the applied electrostatic potential $\varphi(z)$ through $\mathrm{U}_i = -e\varphi(z_i)$, where e is the electronic charge and z_i the vertical position of the i-th layer. The electrostatic potential is obtained via self-consistently solving the Poisson's equation[5],

$$\frac{d^2\varphi(z)}{dz^2} = -\frac{e\left[\rho_h(z) - \rho_e(z)\right]}{\kappa_{bp}\kappa_0} \tag{S1.5}$$

where $\kappa_{bp} = 8.3$ is the out-of-plane dielectric constant of BP[6], κ_0 is the vacuum permittivity, and ρ_h (ρ_e) denotes hole (electron) carrier density (per unit volume). The latter can be calculated from the eigenenergies, $E_{sj\mathbf{k}}$, and eigenvectors, $\Psi_{sj\mathbf{k}}$, of H.

To speed up the self-consistent calculation, we use a simplified approach based on an approximate separation of the Schrodinger problem in the in-plane and out-of-plane directions.

At each iteration of the self-consistent loop, the eigenvalue problem (independent of **k**) associated with H^s is solved numerically to obtain the eigenvalues E_j^s and normalized eigenvectors (modes) ψ_j^s, with $j \in [1, N]$. We disregard the field-induced coupling between the conduction and valence modes with different indices, as a first-order approximation, so that the full Hamiltonian in (S1.1) can be decoupled into a set of N independent Hamiltonians, one for each pair of conduction and valence modes:

$$\mathrm{H}_j = \begin{pmatrix} E_j^c + \eta^c k_x^2 + \nu^c k_y^2 & \gamma k_x \\ \gamma k_x & E_j^v - \eta^v k_x^2 - \nu^v k_y^2 \end{pmatrix}. \tag{S1.6}$$

Near the subband edges, the dispersion corresponding to (S1.6) is parabolic, $E_{j\mathbf{k}}^c \approx E_j^c + \hbar^2 k_x^2 / 2m_x^{cj} + \hbar^2 k_y^2 / 2m_y^{vj}$, where $m_x^{cj} = \hbar^2 / \left[2\gamma^2 / (E_j^c - E_j^v) + 2\eta_c\right]$ and $m_y^{cj} = \hbar^2 / 2\nu^c$. The corresponding density of states is $\mathrm{D}_j^c = \sqrt{m_x^{cj} m_y^{cj}} / \pi\hbar^2$. To further simplify the problem, we calculate the carrier densities $\rho_{e/h}$ by approximating the eigenvectors as $\Psi_{sj\mathbf{k}} \approx \Psi_{sj\mathbf{0}}$, where $\Psi_{sj\mathbf{0}}$ can be reconstructed as,

$$\Psi_{cj\mathbf{0}} = \begin{pmatrix} \psi_j^c \\ 0 \end{pmatrix}, \Psi_{vj\mathbf{0}} = \begin{pmatrix} 0 \\ \psi_j^v \end{pmatrix}, \tag{S1.7}$$

We get:

$$\rho_e(z_i) = \frac{1}{a_z} \sum_j \mathrm{D}_j^c k_B T \ln\left[1 + \exp\left(\frac{E_F - E_j^c}{k_B T}\right)\right] |\psi_j^c(z)|^2, \tag{S1.8}$$

and similarly for the hole case, where E_F is the Fermi level, $a_z = 0.54\,\mathrm{nm}$ the interlayer distance, k_B Boltzmann's constant, and $T = 300\,\mathrm{K}$ the temperature.

Once convergence is reached, the Hamiltonian in (S1.1) is numerically diagonalized to get exact eigenvalues $E_{sj\mathbf{k}}$ and eigenvectors $\Psi_{sj\mathbf{k}}$. The quantities, $E_{ij} = E_{ci\mathbf{0}} - E_{vj\mathbf{0}}$ and $\mathrm{S}_{ij} = \langle \Psi_{ci\mathbf{0}} | \Psi_{vj\mathbf{0}} \rangle$ are defined in the main text as transition energy and wave function overlap, respectively.

The optical conductivity along the x-axis (AC direction) pertaining to $ci-vj$ transition, is then computed with Kubo formula:

$$\sigma_{ij}(\omega)=\frac{\hbar e^2}{i(2\pi)^2}\int \mathbf{dk}\frac{\left(f(E_{cik})-f(E_{vjk})\right)\left|\langle\Psi_{ci\mathbf{k}}\,|\,\hat{v}_x\,|\,\Psi_{vj\mathbf{k}}\rangle\right|^2}{\left(E_{cik}-E_{vjk}\right)\left(E_{cik}-E_{vjk}+\hbar\omega+i\eta\right)}, \tag{S1.9}$$

.where $\hat{v}_x=\hbar^{-1}\partial \mathrm{H}/\partial k_x$ is the velocity operator along the x-axis and $f(\cdot)$ is the Fermi-Dirac distribution function. η is a phenomenological broadening term to account for finite damping. The x-axis relative permitivity can subsequently be calculated via: $\grave{o}(\omega)=1+i\sigma/\grave{o}_0\omega t_{bp}$, where $\sigma=\sum_{ij}\sigma_{ij}$ and t_{bp} is the BP thickness. It is understood that contributions to σ, due to intraband transitions are negligible in the energy range of interest. The optical transfer matrix method is used to compute the transmission spectra for the geometry shown in Fig. 1a of the main text. The refractive indices for Al_2O_3 (10 nm), SiO_2 (450 nm), and Si are taken from Ref. [7].

2. ***Measurement Setup*** ---The measurement setup used in this study is schematically shown in Fig. S1. An optical parametric oscillator (Firefly-IR, M Squared) with a tunable output wavelength range from 2.5 to 3.7 um is used in the measurement. The output mid-infrared light is split to a signal beam and a reference beam. Signal and reference beams are chopped by the

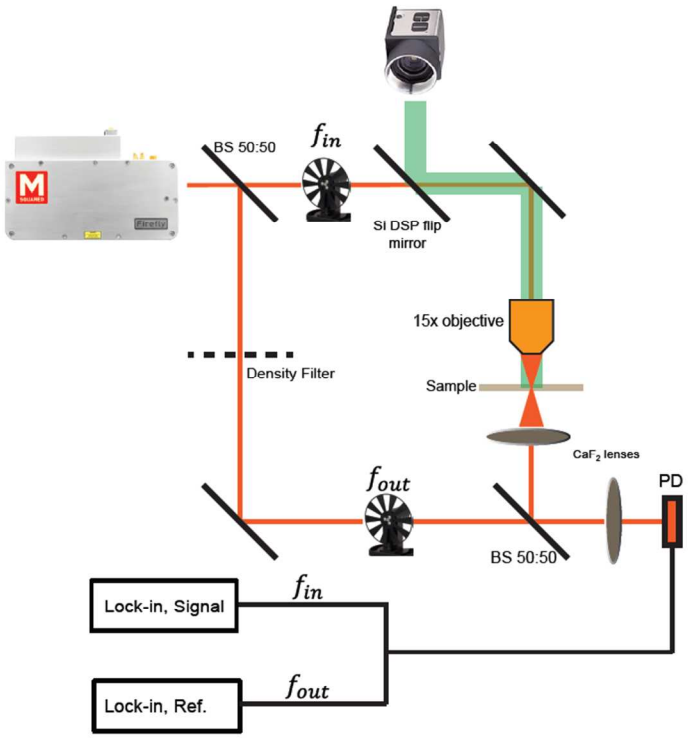

Figure S1. Schematics of the mid-infrared BP modulation measurement setup.

inner and the outer part of the chopper which has different duty cycle. Therefore, the two beams are chopped at different frequencies to be differentiated. The signal beam is focused on the sample by a 15x objective to a spot of 20 μm in diameter which is smaller than the sample size. The transmission light of the signal beam is collected by the CaF2 lenses and focus on a InAsSb photodetector (PD). The photodetector current is measured by a lock-in amplifier and the transmitted optical power is calculated. For the reference beam, the power is measured by the same photodetector connected to another lock-in amplifier locked to a different chopper frequency from that of the signal beam. In addition, a density filter in the path of the reference beam is used to balance the power of signal beam and reference beam. The relative transmission of the signal beam power is thus calculated by normalizing to the reference beam power. In this way, the temporal fluctuation of the laser power and its variation during the wavelength scan is canceled out. By using this setup and averaging the measurement data, the accuracy of the measurement of the transmission can be better than 10^{-3}.

3. *Fabrication Method* --- Fig. S2 illustrate the device fabrication process. The BP modulators were fabricated on Si wafer with 450 nm top SiO_2 layer. First, the SiO_2 layer was grown on the Si substrate using an atmosphere oxidation system (TYLAN Furnace) and used as gate dielectric materials. Then the SiO2 layer was patterned using photolithography technique with S1813 photoresist and etched with buffered oxide etchant (BOE) through to reach the bottom silicon substrate. Electron-beam evaporation was then used to deposit 5 nm Ti/ 50 nm Au back gate electrode using the remaining photoresist as a mask. After removing the resist in N-methylpyrrolidone (NMP), BP thin film was exfoliated from bulk crystal and transferred onto the substrate by standard dry transfer method using a PDMS stamp. After the transfer, a layer of photoresist were immediately spun on to cover the BP film to prevent oxidation. Then the source and drain electrodes were patterned and deposited with 5 nm Ti/ 50 nm Au. After lift-off process, 10 nm Al2O3 was grown by ALD system to passivate the surface of BP.

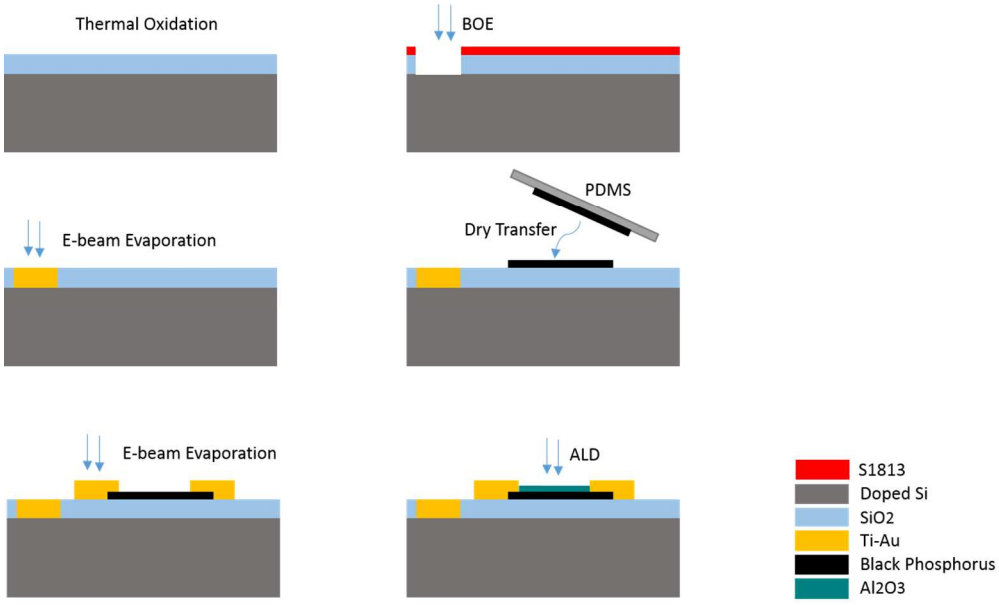

Figure S2. Fabrication process of mid-IR BP modulator.

S4. *Electrical Characterization*

We have also performed the I_{ds}-V_g measurement as shown in Fig. S3. It confirms that the BP is initially p-doped. Although the plot shows a minimum transconductance at ~+80V, it does not necessarily mean the Fermi level is at the neutral because the source and drain contacts made of gold has a Schottky barrier to the BP. Instead, the gate voltage modulation on the Schottky barrier height at the contacts can play a dominant role on the transconductance[8].

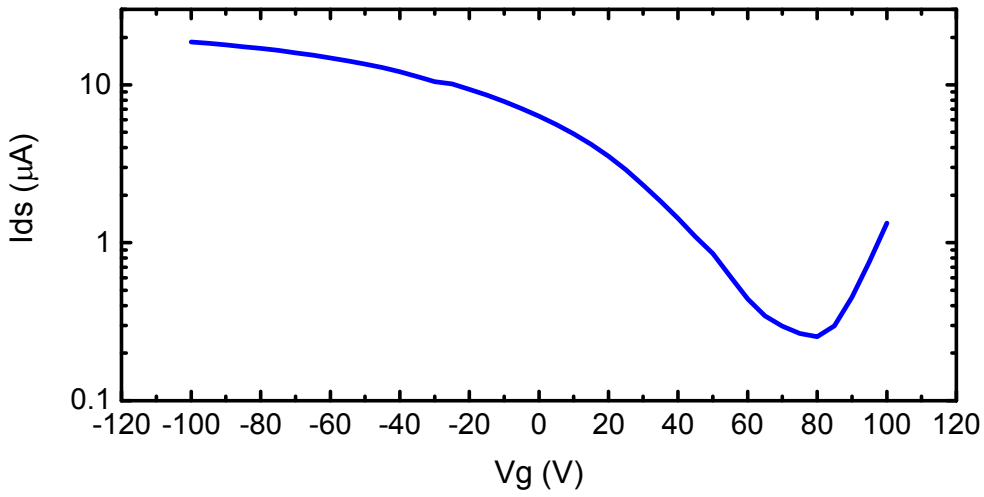

Figure S3 Source-drain current I_{ds} versus back gate voltage V_g of the 9 nm thick BP device.

S4. ***More devices with different BP thickness*** --- We have fabricated several devices with BP flakes of different thickness and performed the same measurement as for the device with 9nm BP in the main text. In Figure 4 of the main text, the positions in energy of the modulation peaks were extracted from the 2D contour plots of the devices. As shown in Fig. S4. We extracted the modulation peaks at different gate voltages and interpolated to the zero gate voltage condition. Compared with the 9nm devices, more modulation peaks and features are observed in thicker devices, as expected from theory. Particularly in a 13 nm device (Fig. S4b), more than 5% modulation in transmission was observed, which show great potential for an integrated BP modulator operating in the mid-infrared.

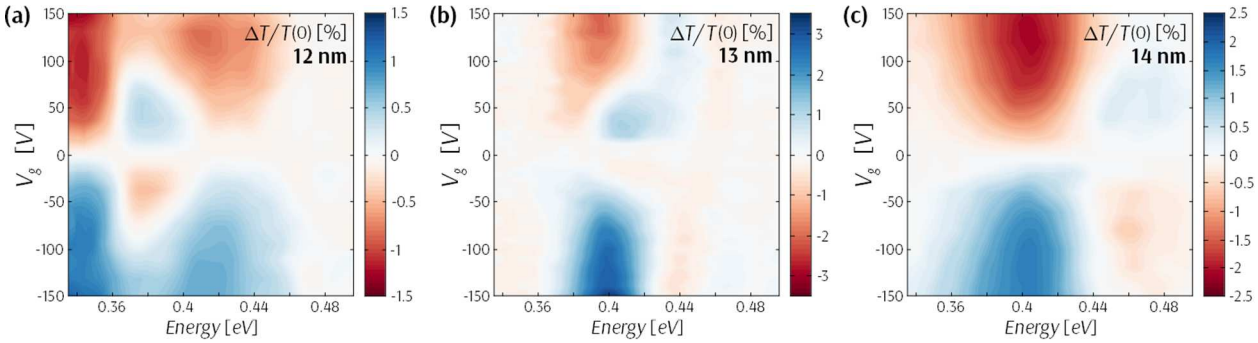

Figure S4 2D modulation mapping of three other devices with different BP thickness.

Theoretical study in the main text (Figs. 2 and 3) is restricted to the 9 nm thick BP, the thinnest device in our study, as it has only 5 sub-band optical transitions that contributes to the energy measurement window of interest. Here, the sub-band energies are *well-spaced*, hence allowing us to resolve the different optical transitions reliably. In thicker samples, more sub-bands take part in the absorption spectrum within our measurement window, and the energy separation between the sub-bands are also smaller, which further complicates the analysis. In particular, it is well known that trapped charges at oxide interfaces can lead to charge inhomogeneity (~1×10^{12} cm^{-2}) in 2D materials, hence spatial variations in the potential energy landscape (~50 meV). Hence, the device with larger thickness simply does not have the "energy resolution" for us to reliably resolve these optical transitions within our simplified disorder-free model. Despite of this, the main two relations developed based on the case of 9 nm thick BP, namely (1) the

connection between the inter-subband transitions and the extremum observed in the modulation level and (2) the sign variation of modulation level with the back-gate voltage polarity and its relationship with how same-indexed and hybrid transitions depend on bias, can be used to *qualitatively* explain the modulation level in thicker samples. For instance, with increasing hole density, the negative-to-positive sign variation in 13 nm thick sample at around 0.41 eV can be related to same-indexed transitions while for the reverse sign change around 0.44 eV hybrid transitions ought to play the main role.

References

1. Rodin, A.; Carvalho, A.; Neto, A. C. *Phys. Rev. Lett.* **2014,** 112, 176801.
2. Low, T.; Roldán, R.; Wang, H.; Xia, F.; Avouris, P.; Moreno, L. M.; Guinea, F. *Phys. Rev. Lett.* **2014,** 113, 106802.
3. Low, T.; Rodin, A.; Carvalho, A.; Jiang, Y.; Wang, H.; Xia, F.; Neto, A. C. *Phys. Rev. B* **2014,** 90, 075434.
4. Zhang, G.; Huang, S.; Chaves, A.; Song, C.; Ozcelik, V. O.; Low, T.; Yan, H. *Nat. Commun.* **2017,** 8, 14071.
5. Stern, F. *J. Comput. Phys*. **1970,** 6, 56-67.
6. Morita, A. *Applied Physics A: Materials Science & Processing* **1986,** 39, 227-242.
7. Polyanskiy, M. N., Refractive index database https://refractiveindex.info.
8. Penumatcha, A. V.; Salazar, R. B.; Appenzeller, J. *Nat. Commun.* **2015,** 6.